Supporting Information

Nanoimprint lithography-assisted block copolymer self-assembly for hyperfine fabrication of magnetic patterns based on $L1_0$-FePt nanoparticles

Jie Zhang [a,b], Yi Chen [c], Guijun Li [c], Zelin Sun [a,b*] Zhengong Meng [a,d]*, Wai-Yeung Wong [a,b]*

[a] Department of Applied Biology and Chemical Technology and Research Institute for Smart Energy, The Hong Kong Polytechnic University, Hong Kong, China.

[b] The Hong Kong Polytechnic University Shenzhen Research Institute, Shenzhen 518057, China

[c] Division of Integrative Systems and Design, and Department of Electronic and Computer Engineering, The Hong Kong University of Science and Technology, Hong Kong, China

[d] School of Flexible Electronics (Future Technology) and Institute of Advanced Materials (IAM), Nanjing Tech University, 30 South Puzhu Road, Nanjing 211800, China

1. Materials and instruments

1.1 General

All reactions were carried out under nitrogen unless otherwise stated. Commercially available reagents were used without further purification. All reactions were monitored by thin-layer chromatography (TLC) with Merck pre-coated glass plates. Separation or purification of products was achieved by column chromatography or preparative TLC using silica gel from Merck (230-400 mesh). ^{1}H and ^{13}C NMR spectra were recorded on a Bruker AVANCE III 400 MHz FT-NMR spectrometer. Data treatment was performed with software MestReNova. The chemical shift values (δ) were referenced to the residual solvent peaks in the unit of ppm. Coupling constants (J) were reported in the unit of hertz (Hz). Chemical shifts were referenced against tetramethylsilane as the internal standard for ^{1}H and ^{13}C NMR data. The structure and surface functionalities of the precursors were explored through the fourier-transform infrared spectroscopy (FTIR). High resolution mass spectra were recorded using a Bruker UltrafleXtreme matrix-assisted laser desorption ionization time-of-flight (MALDI-TOF) mass spectrometer along with FlexAnalysis software.

Nanostructure Characterization. The structural characterization of the as-synthesized FePt NPs was performed by PXRD on a Rigaku Smart Lab 9 kW X-ray diffractometer, with Cu $K_{\alpha 1}$ (λ = 540 nm, 40 kV, 30 mA) for analyzing the

composition and phase purity of the resulting NPs. TEM was performed on a JEOL Model JEM-2100F field emission electron microscope, with copper grids as substrates for probing the morphology, particle size and size distribution of NPs. SEM characterizations of self-assembled nanostructures were performed on a Tescan MAIA3 field emission scanning electron microscope, and a Tescan VEGA3 scanning electron microscope was used for EDX analysis to study the ratio of Fe and Pt in the resulting metal alloy NPs. The magnetic hysteresis loop at room temperature was measured by a physical property measurement system (PPMS).

1.2 Materials

Ferrocenecarboxaldehyde, sodium borohydride, sodium hydroxide, 4-bromobenzyl bromide, isopropylmagnesium chloride, XPhos, $Pd_2(dba)_3$, Na_2CO_3, K_2CO_3, K_2PtCl_4 and block copolymers PS-*b*-P4VP were procured from various suppliers: Sigma-Aldrich, Energy, Dieckmann, and Polymer Source. These chemicals were utilized as received, without any additional purification processes. The separation or purification of products was performed using column chromatography or preparative TLC, utilizing silica gel procured from DAVISIL® (particle size 70-200 μm) or aluminium oxide.

1.3 Detailed synthesis procedure of the metallic block copolymer

Preparation of ferrocenylmethanol (1)

A certain amount of ferrocenecarboxaldehyde (1 equiv.) was dissolved in ethanol and the solution was cooled down to the desired temperature in an ice bath. Subsequently, the predetermined sodium borohydride (5 equiv.) in sodium hydroxide was dropwise added into the system. The resultant solution was put overnight to reach complete reaction, and the orange solid product could be successfully extracted with nearly 90% yield after post-treatment. ^{1}H NMR (400 MHz, DMSO-d_6): δ 4.73 (s, 1H, -OH), 4.24-4.16 (m, 4H, ferrocenyl), 4.13 (s, 5H, ferrocenyl), and 4.08 (t, J = 2.0 Hz, 2H, -CH_2-O). ^{13}C NMR (100 MHz, $CDCl_3$): δ 88.75, 77.35, 77.03, 76.72 (ferrocenyl), and 68.51 (ferrocenyl-C-O).

Preparation of 1-((ferrocenyloxy)methyl)-4-bromobenzene (2)

The reactant 1 (1.22 g, 5.65 mmol, 1.14 equiv.) was dissolved in DMF (40 mL) in an ice bath and NaH (142.83 mg, 60% in mineral oil, 5.95 mmol, 1.2 equiv.) was added into the stirred solution. Then, the mixture was warmed to room temperature while stirred for 30 min, then cooled to 0 ℃. After 4-bromobenzyl bromide (1.24 g, 4.96 mmol, 1 equiv.) was added, the reaction mixture was warmed to room

temperature, stirred for 2 h, and quenched with saturated aqueous NH_4Cl solution. The mixture was extracted with Et_2O, and then the organic layer was washed with DI water for four times and dried over Na_2SO_4. After evaporation of the solvent, the crude mixture was purified by silica gel column chromatography (hexane/ethyl acetate = 20/1 to 10/1, v/v) and the orange solid product could be successfully extracted with 70% yield. ^{1}H NMR (400 MHz, $CDCl_3$): δ 7.51-7.42 (m, 2H, Ar), 7.24-7.17 (m, 2H, Ar), 4.45 (s, 2H, -CH_2-O), 4.31 (s, 2H, -CH_2-O), 4.23 (t, J = 1.8 Hz, 2H, ferrocenyl), 4.16 (t, J = 1.9 Hz, 2H, ferrocenyl), and 4.12 (s, 5H, ferrocenyl). ^{13}C NMR (100 MHz, $CDCl_3$): δ 137.75, 131.72, 131.59, 129.50, 129.44, 121.45 (Ar), 83.30, 77.48, 76.84, 70.99 (ferrocenyl), 69.56 (ferrocenyl-C-O), and 68.61 (Ar-C-O).

Preparation of the 2-heterocyclic organozinc reagent (3)

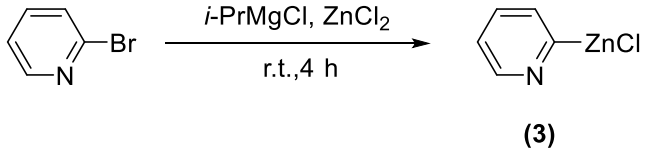

(3)

Figure S1 Synthetic route for the 2-heterocyclic organozinc reagent.

An oven-dried Schlenk bottle equipped with a magnetic agitator was first utilized to contain 2 M isopropylmagnesium chloride in THF (2.75 mL, 5.5 mmol, 1.1 equiv.), followed by dropwise addition of 2-bromopyridine (0.789 g, 5 mmol, 1 equiv) in an ice bath. The resultant solution was stirred for 4 h at ambient temperature under nitrogen

protection. Subsequently, 2 M $ZnCl_2$ in anhydrous THF (12 mL, 6 mmol, 1.2 equiv) was added and the mixture was continuously stirred for another 1 h in the ice bath. The mixture was further employed for the Negishi cross-coupling without further purification.

2. TEM and SAED of $L1_0$-FePt NPs

The morphologies and size distribution of the obtained FePt NPs were examined by TEM at low and high resolution, respectively. **Figure S2** shows the TEM images of FePt NPs, which were synthesized through the pyrolysis of metallic precursor P1. As shown in the low-resolution TEM images, the obtained FePt alloy NPs exhibited uniform shapes. The NPs were evenly dispersed onto the amorphous carbon matrix, where the carbonaceous substrate could immobilize and protect the FePt alloy NPs from self-aggregation and oxidation under an anaerobic environment. Also, an amorphous carbon structure could be discerned around the NPs.

The high-resolution TEM (HRTEM) image (**Figure S2b**) of NPs pyrolyzed from P1 showed the crystalline spacing of the FePt NPs. The measured crystalline spacing was calculated to be 0.2 nm, which was assigned to the (111) plane of FePt alloy as reported in the literature. The measured crystalline spacing of the FePt NPs was calculated to be 0.23 nm, which was assigned to the (200) plane of FePt alloy reported in the literature.[1] This result implied that the resultant FePt-NPs were highly ordered and consisted of a $L1_0$ phase. The size distribution of the obtained FePt NPs was statistically analyzed based on the TEM image in **Figure S2d**. Counting over 50 of the FePt NPs, the average diameter of the resultant FePt NPs was calculated to be 7.11 nm. The sizes of particles showed a uniform distribution and thus a desired SNR for the data

readback in magnetic recording devices could be expected.

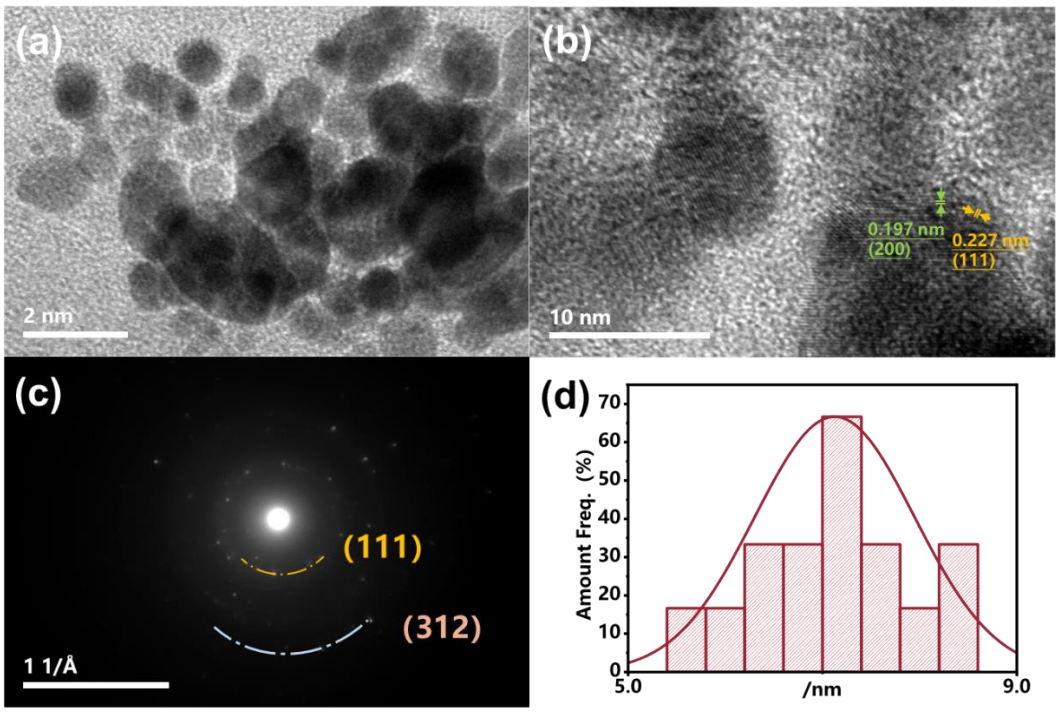

Figure S2 (a) Low-resolution TEM image; (b) HRTEM image; (c) SAED image and (d) diameter distribution of FePt NPs derived from the pyrolysis of P1.

TEM and SAED studies were also conducted on the characteristics and dimensions of the FePt NPs derived from the pyrolysis of P2, as shown in **Figure S3**. The lower-resolution TEM images illustrate uniformity in the shapes of the FePt alloy NPs. The NPs were also surrounded by an identifiable amorphous carbon structure.

The HRTEM depiction in **Figure S3b** of the resultant FePt NPs provides an insight into the crystalline structure of the FePt NPs. The calculated interplanar spacing is 0.22 nm in concordance with the (111) plane of the FePt alloy. Additionally, a

calculated interplanar spacing of 0.19 nm corresponds to the (200) plane of the FePt alloy. This analysis reveals that the synthesized FePt NPs exhibit a highly structured nature, indicative of a predominant $L1_0$ phase. The SAED, as depicted in **Figure S3c**, further substantiates the findings pertaining to the crystal orientation and lattice constants of the synthesized NPs. It affirms the conformity between the produced NPs and the $L1_0$ plane of the FePt NPs, as previously reported in the literature.[2] The size distribution of the synthesized FePt NPs was statistically evaluated, referencing the TEM representation in **Figure S3d**. The mean diameter was calculated to be 6.99 nm. The size of the NPs was observed to be smaller than that of FePt NPs derived from the pyrolysis of P1.

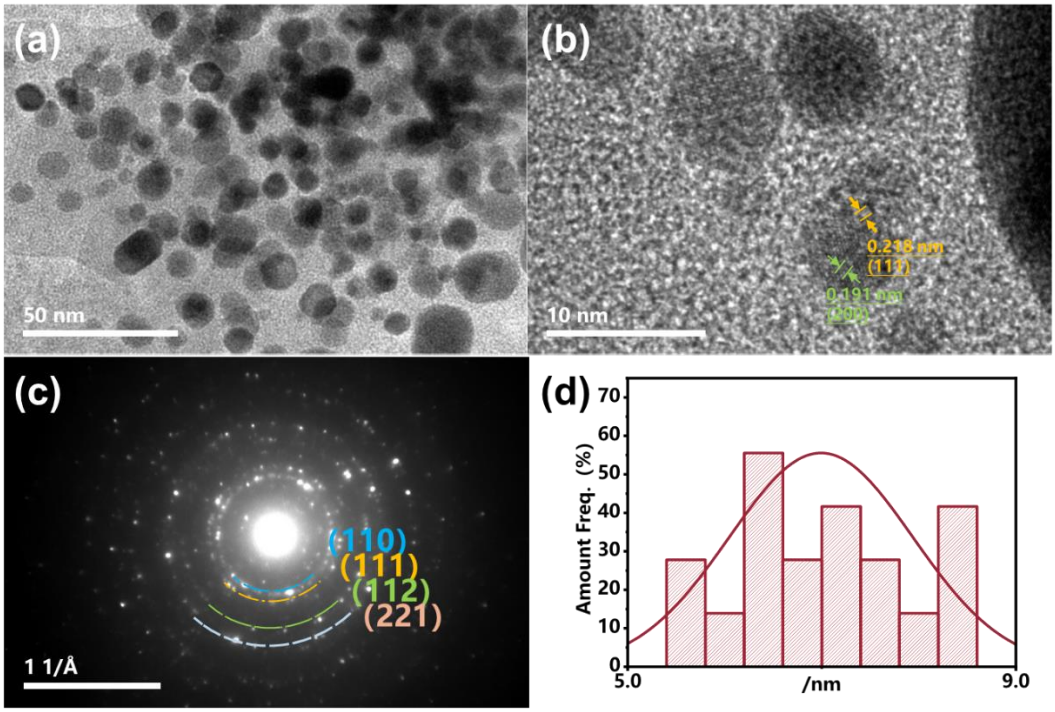

Figure S3 (a) Low-resolution TEM image; (b) HRTEM image; (c) SAED image and (d)

diameter distribution of FePt NPs derived from the pyrolysis of P2.

An exploration into the properties and dimensions of FePt NPs derived from the pyrolysis of P4 was undertaken by employing TEM. **Figure S4** shows the TEM and SARD results of the **FePt NPs** resulting from the pyrolysis of P4. As evidenced by the low-resolution TEM image, the FePt alloy NPs exhibit consistency in their form. As obtained in **Figure S4b**, the crystal lattice spacing was 0.21 nm, aligning with the (111) plane of the FePt alloy. A crystal spacing of 0.20 nm was observed, corresponding to the (200) plane of the FePt alloy. The findings suggest that the engineered FePt NPs are significantly organized and comprise of the $L1_0$ phase. The SAED results, displayed in **Figure S4c**, substantiate the evidence relating to the synthesized NPs' crystal orientation and lattice constants. This affirms the congruity between the synthesized NPs and the $L1_0$ plane of the FePt NPs, as reported in prior studies. The size distribution of the produced FePt NPs was assessed statistically, referencing to the TEM illustration in **Figure S4d.** The calculated mean diameter amounted to 4.34 nm. As designed, FePt NPs derived from the pyrolysis of P4 are found to be the smallest, which can be credited to the extended carbon chain length of the P4 precursor in comparison to the other precursors. These results further suggest that the longer the carbon chain of the precursors, the smaller the NPs.

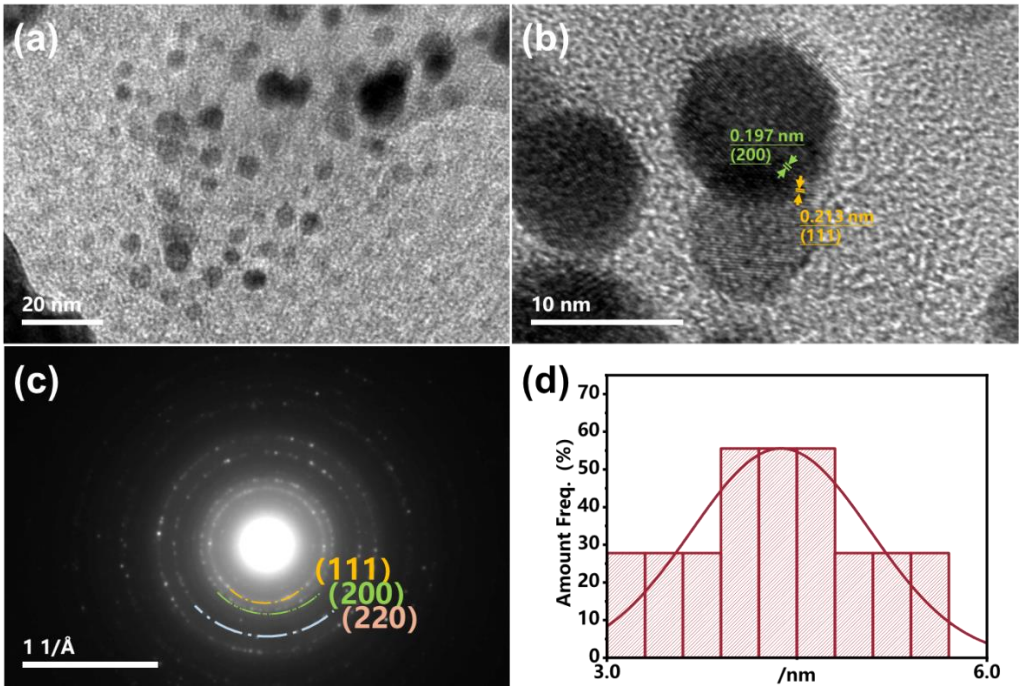

Figure S4 (a) Low-resolution TEM image; (b) HRTEM image; (c) SAED image and (d) diameter distribution of FePt NPs derived from the pyrolysis of P4.

3. PXRD of $L1_0$-FePt NPs

Figure S5 shows the PXRD spectrum of FePt NPs acquired through the pyrolysis of P1 using Cu Kα radiation. The sharp and well-defined diffraction peaks, align with the standard peaks of FePt alloys as documented in the JCPDS Card no. 043-1359. Specifically, this PXRD diagram for FePt NPs reveals identifiable diffraction peaks of the (001) and (110) at 22^o and 32^o. These peaks are typical superlattice peaks of the $L1_0$ phase of FePt NPs, conclusively demonstrating that the synthesized FePt NPs possess a chemical order characteristic of the $L1_0$ phase.

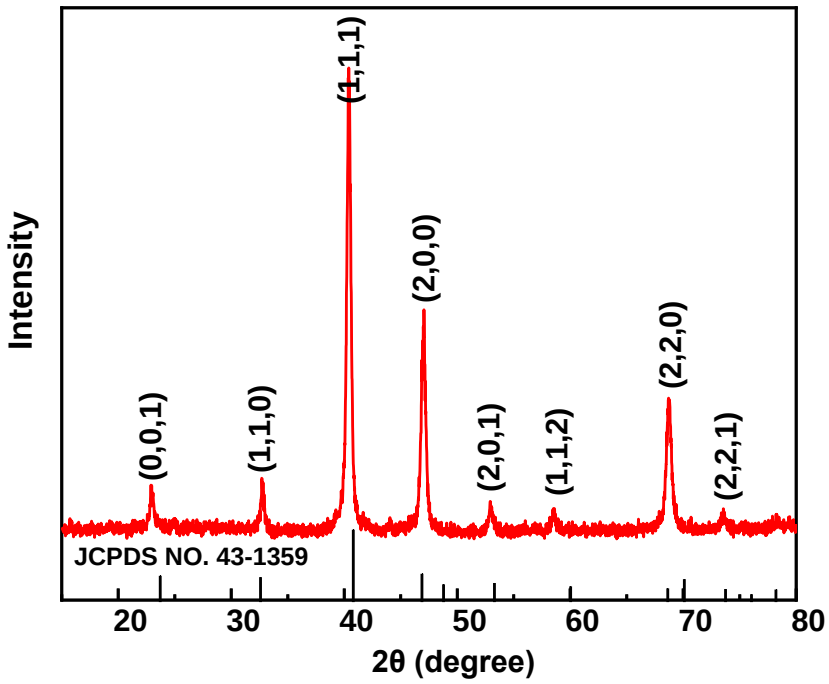

Figure S5 PXRD spectrum of FePt NPs derived from the pyrolysis of P1.

The PXRD spectrum for NPs generated from the pyrolysis of the metallic precursor P2 is depicted in **Figure S6**. The diffraction signatures for the resultant FePt NPs exhibit characteristic superlattice diffraction peaks, specifically at the (111) and (110) planes. These signatures are also commensurate with a face-centered tetragonal (fct) structure of FePt NPs. Also, the dominant (111) peaks can also be found in the HRTEM image with the 0.22 nm of the crystallites. Thus, the findings demonstrate that the FePt NPs created in this process exhibit a high degree of chemical order in the $L1_0$ phase.

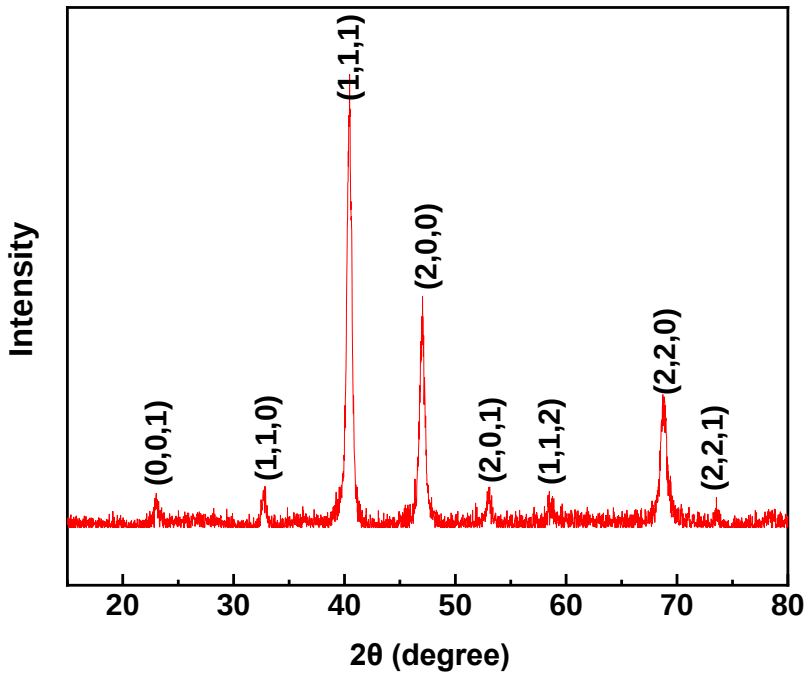

Figure S6 PXRD spectrum of FePt NPs derived from the pyrolysis of P2.

The PXRD pattern of the FePt NPs derived from the pyrolysis of P4, as shown in **Figure S7**, exhibits distinct diffraction peaks. These peaks match with the standard FePt peaks as referenced by the JCPDS card number 043-1359. The formation of a chemically ordered face-centered tetragonal structure for NPs is affirmed by the marked (001) and (110) peaks.

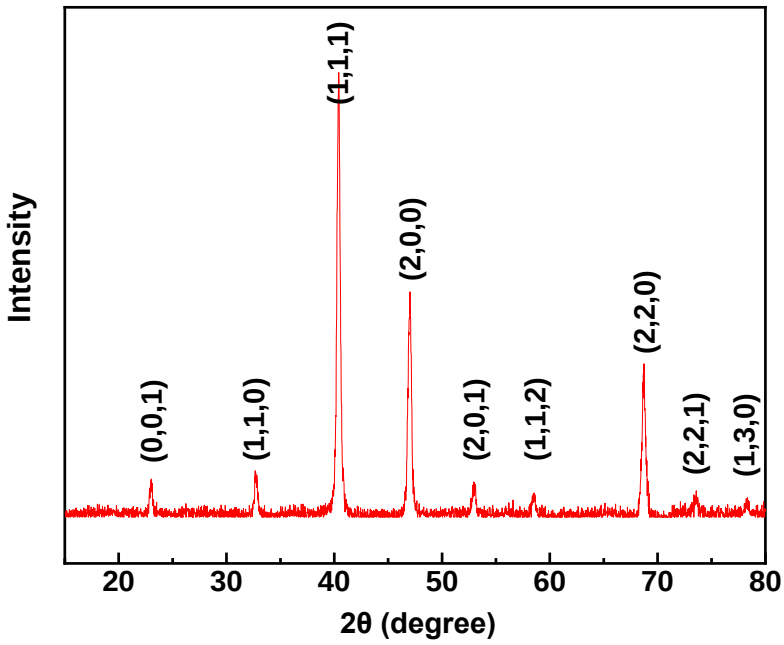

Figure S7 PXRD spectrum of FePt NPs derived from the pyrolysis of P4.

References

[1] Meng Z, Li G, Wong HF, Ng SM, Yiu SC, Ho CL, Leung CW, Manners I, Wong WY. *Nanoscale*, 2017, 9: 731-738.

[2] Meng Z, Xiao F, Wei Z, Guo X, Zhu Y, Liu Y, Li G, Yu ZQ, Shao M, Wong WY. *Nano Res.*, 2019, 12: 2954–2959.